

Effectively nonlinear magneto-optical detection under strong laser fields

Chen Qian,^{1,2} and Ruifeng Lu^{1,*}

¹ *Institute of Ultrafast Optical Physics, MIIT Key Laboratory of Semiconductor Microstructure and Quantum Sensing, Department of Applied Physics, Nanjing University of Science and Technology, Nanjing 210094, P R China*

² *Institute of Physics, Chinese Academy of Sciences, Beijing National Laboratory for Condensed Matter Physics, Beijing 100190, P R China*

Abstract

We report a strong-field detection method for magnetic materials, based on the characterization of crystal time-reversal symmetry through the elliptical dichroism of harmonics. The consistency of the low-order harmonics driven by laser fields with opposite helicities originates from the time-reversal symmetry of crystals, and thus the appearance of harmonic elliptical dichroism can serve as evidence for the breaking of crystal time-reversal symmetry. We have used the semiconductor Bloch equation to calculate the harmonic spectra of the bilayer ferromagnetic material $\text{Cr}_2\text{Ge}_2\text{Te}_6$, with and without spin-orbit coupling. In magnetic materials, strong spin-orbit coupling causes the loss of time-reversal symmetry in the phase of polarization currents between different spin states, inducing elliptical dichroism in the harmonics. Here we extend the magneto-optical Faraday or Kerr effect to the nonlinear domain using strong laser fields, improving the sensitivity and applicability of magneto-optical detection methods.

Harmonic generation (HG) under the strong laser field encode the fundamental information of the electronic states in crystals, such as symmetry, topological properties, and correlated interactions [1-10]. Laser fields with different helicities can selectively excite electron spin, valleys, and chirality [11-14]. Understanding the correspondence between the rule of harmonics and the characteristic of electronic states can help us deconstruct material properties using all-optical methods. Solid-state HG have long been an effective detection technique, satisfying the selection rules established by the crystal point-group symmetry [2,3]. However, the laws governing strong-field optical effects in magnetic space and with strong spin-orbit coupling have not been clarified [15]. Here, a strong-field method for detecting magnetic materials via harmonic elliptical dichroism is introduced.

The current means of magnetism detection primarily relies on the macroscopic magnetization of materials, rather than the time-reversal symmetry itself, which brings some technical challenges. Traditional magnetic detection methods, such as magnetic hysteresis loop or magnetic circular dichroism [16-19], require the application of an external magnetic field to align the spins for detection, which to some extent disrupts the intrinsic spin polarization of materials. Furthermore, for antiferromagnets, due to the absence of a net magnetic moment, they are considered difficult to be directly detected by linear optical techniques like the magneto-optical (MO) Faraday and Kerr

* rflu@njust.edu.cn

effects [20-22]. Therefore, investigating the intrinsic time-reversal symmetry is crucial for the characterization of magnetic materials. Second-harmonic generation (SHG) is highly sensitive to both the crystallographic structure and magnetic order [23-27], but it cannot be obtained through the electric dipole effect in centrosymmetric systems, and its exact origin is difficult to determine in non-centrosymmetric systems, which largely limits its use as a sufficient condition for judging the magnetism [24]. Therefore, under stronger laser field conditions, utilizing the third-order or even higher-order optical responses to reveal the crystal symmetry becomes particularly important.

We generalize MO Faraday and Kerr effects to the nonlinear domain to directly detect the time-reversal symmetry of materials using the elliptical dichroism of harmonics, without the assistance of an external magnetic field. In previous researches on non-magnetic semiconductors, it is found that the intensities of low-order harmonics generated by left-circularly and right-circularly polarized laser fields are almost consistent [28,29]. Now we clarify that this rule is broken in magnetic materials, due to the breaking of time-reversal symmetry. The ellipticity dependence of low-order HG in h-BN and the Haldane model has been discussed [3], where the participation of a magnetic phase led to a significant difference in the elliptical dichroism of harmonics. In this work, our discussion will be further extended to intrinsic magnetic materials.

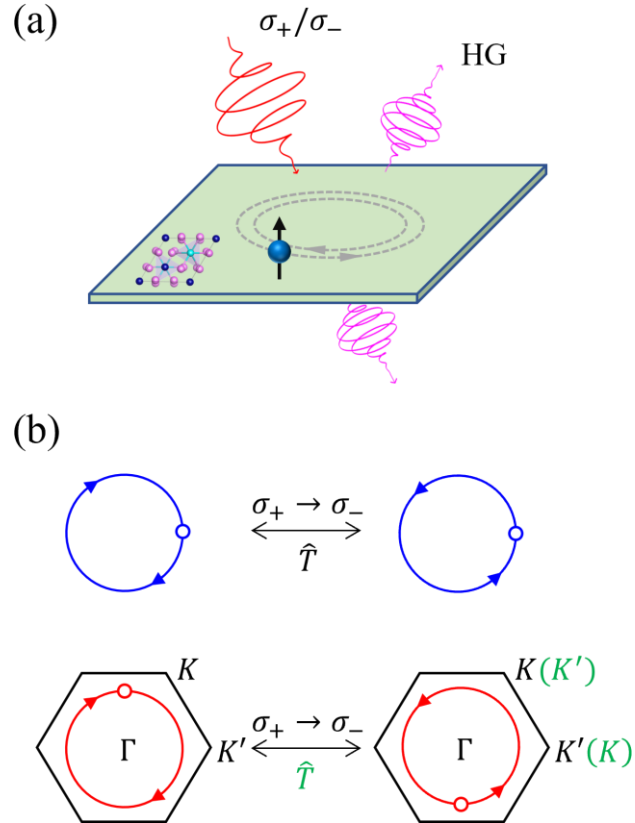


FIG. 1. (a) Circularly polarized light drives the in-plane spin electron motion in two-dimensional magnetic materials, generating harmonic radiation. (b) Time reversal causes the helicity flipping of the electric field (blue) and vector potential (red) of lasers. The small white circles represent the position at time 0. The time reversal of high symmetry \mathbf{k} points are marked with green.

Circularly polarized laser fields and the motion of spin-polarized electrons both possess chirality. Driving spin-polarized electrons with a periodic circularly polarized laser field can induce laser-helicity sensitive electron motion, and which results in HG with dichroism [Fig. 1(a)]. The circular dichroism of harmonics can be applied to detect chiral molecules or crystals, as well as the spin polarization of electrons associated with the chirality.

Applying the time-reversal symmetry operation \hat{T} to a circularly polarized laser field confined in the two-dimensional plane is equivalent to flipping its helicity. As shown in Fig. 1(b), the laser electric field has $\hat{T}\mathbf{E}_{\sigma_+}(t) \rightarrow \mathbf{E}_{\sigma_-}(-t) = \mathbf{E}_{\sigma_+}(t)$, vector potential has $\hat{T}\mathbf{A}_{\sigma_+}(t) \rightarrow \mathbf{A}_{\sigma_-}(-t) = -\mathbf{A}_{\sigma_+}(t)$, (σ_+ right-hand helically, σ_- left-hand helically), and the reciprocal lattice has $\hat{T}\mathbf{k}(t) \rightarrow \mathbf{k}(-t) = -\mathbf{k}(t)$. When \hat{T} is applied to the whole laser-crystal system, according to Neumann's principle, for crystals with time-reversal symmetry, the photocurrent induced under a helically polarized laser field should satisfy the time-reversal symmetry that $\hat{T}\mathbf{J}_{\sigma_+}(t)\hat{T}^\dagger \rightarrow \mathbf{J}_{\sigma_-}(-t) = -\mathbf{J}_{\sigma_+}(t)$.

Thus, harmonic spectra of non-magnetic materials ought to satisfy $I_{\sigma_-}(\omega) = I_{\sigma_+}(\omega)$, which means there is no harmonic elliptical dichroism. However, due to the accumulation of charge carriers in the crystal and the thermal effect between particles, this requirement can only be satisfied under appropriate conditions, especially in real materials.

Under the strong laser field, the magnetic dipole effect is relatively weak, the polarization current between two bands under the electric dipole approximation can be written as

$$\begin{aligned} \mathbf{J}_{nm}[\mathbf{k}(t), t] &= \rho_{nm}[\mathbf{k}(t), t] \mathbf{p}_{nm}[\mathbf{k}(t)] \\ &= \int_{-\infty}^t dt' f_{nm}[\mathbf{k}(t), t] \varepsilon_{nm}[\mathbf{k}(t)] |\mathbf{d}_{nm}[\mathbf{k}(t)]| \{ \mathbf{E}(t') \cdot |\mathbf{d}_{mn}[\mathbf{k}(t')]| \} e^{iS_{nm}[\mathbf{k}(t), t, t']}, \end{aligned} \quad (1)$$

where n, m are band indexes. ρ_{nm} and \mathbf{p}_{nm} are the density and momentum matrix elements of electrons, respectively. $f_{nm} = \rho_{nn} - \rho_{mm}$ is the electron density difference between the bands. ε_{nm} and \mathbf{d}_{nm} are the energy difference and the transition dipole moment between bands n and m . S_{nm} is the phase of the polarization current, which in sequence consists of the dynamic phase, the shift phase and the Δ TDP, respectively, as

$$S_{nm}[\mathbf{k}(t), t, t'] = \int_{t'}^t \varepsilon_{nm}[\mathbf{k}(\tau)] d\tau + \int_{t'}^t \mathbf{E}(\tau) \cdot \mathbf{R}_{nm}[\mathbf{k}(\tau)] d\tau + S_{\Delta\text{TDP}}, \quad (2)$$

\mathbf{R}_{nm} is the shift vector, $S_{\Delta\text{TDP}}$ is the phase difference between transition dipoles along the photocurrent and the laser field.

It has been recently proven that the current phase S_{nm} reverses sign under time-reversal symmetry [3], and the polarization current generated by circularly polarized laser has

$$\hat{T} \mathbf{J}_{nm,\sigma_+}[\mathbf{k}(t), t] \hat{T}^\dagger \rightarrow \mathbf{J}_{nm,\sigma_-}[-\mathbf{k}(t), -t] = -\mathbf{J}_{nm,\sigma_+}^*[\mathbf{k}(t), t] \frac{f_{nm}[-\mathbf{k}(t), -t]}{f_{nm}[\mathbf{k}(t), t]}. \quad (3)$$

The electron density difference f_{nm} is responsible for high-order harmonics produced by carrier injection and recollision. However, in the perturbative regime where the photon energy is below the bandgap (ε_g), the interband harmonics mainly stem from the time-dependent evolution of the electron momentum \mathbf{p}_{nm} , rather than the variation of electron density. Therefore, the harmonic spectrum below the bandgap typically satisfies

$$I_{\sigma_+}(\omega) = I_{\sigma_-}(\omega), \omega < \varepsilon_g/\hbar. \quad (4)$$

Our theoretical calculations are carried out in the bilayer $\text{Cr}_2\text{Ge}_2\text{Te}_6$, a two-dimensional intrinsic ferromagnetic material. The layered structure of $\text{Cr}_2\text{Ge}_2\text{Te}_6$ has been verified both theoretically and experimentally. Using a scanning MO Kerr effect microscope, its intrinsic long-range ferromagnetic order in the atomic layers has been detected, breaking the long-established Mermin-Wagner theorem. The pristine $\text{Cr}_2\text{Ge}_2\text{Te}_6$ atomic layer is a near-ideal two-dimensional Heisenberg ferromagnet, and therefore it will be helpful for the development of new-generation magnetic memory storage materials or for studying the fundamental spin behavior of electrons in crystals. However, the MOKE measurement on bilayer $\text{Cr}_2\text{Ge}_2\text{Te}_6$ only shows a few millidegrees, more evidence is needed for its intrinsic magnetism [20].

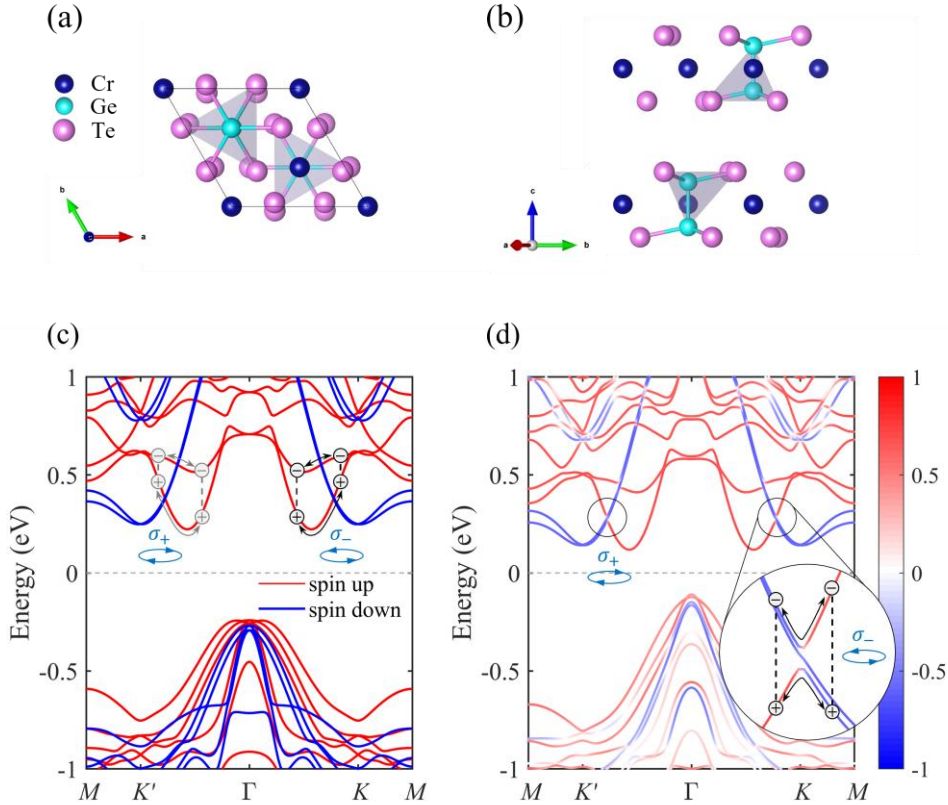


FIG. 2. (a) Top view and (b) side view of the crystal structure of the bilayer AB-stacked $\text{Cr}_2\text{Ge}_2\text{Te}_6$. Band structures of $\text{Cr}_2\text{Ge}_2\text{Te}_6$ (c) without spin-orbit coupling (SOC) and with SOC, z-component spin polarization is indicated by different colors. The black arrows mark the polarization paths of dipoles (positive and negative charge pairs) driven by laser fields with opposite helicities.

The top and side views of the crystal structure of the bilayer $\text{Cr}_2\text{Ge}_2\text{Te}_6$ are shown in Figs. 2(a) and 2(b), respectively. The rhombic box represents the primitive cell, which contains 4 Cr atoms, and each Cr atom is connected to 6 nearest-neighbor Te atoms and is located at the center of the octahedron formed by these Te atoms (the shaded gray regions). Each layer consists of a honeycomb lattice of Cr atoms, similar to graphene, and contains a Ge-Ge metallic bond. The bilayer $\text{Cr}_2\text{Ge}_2\text{Te}_6$ contains two layers stacked in an AB order. According to the structural optimization, the vdW interlayer spacing of the bilayer is around 3.437 Å, and the lattice constant is 6.838 Å [30].

Our first-principles calculations are based on Density Functional Theory (DFT) and performed using the Vienna ab initio simulation package (VASP) [31]. The generalized gradient approximation (GGA) with the Perdew-Burke-Ernzerhof (PBE) functional form is used to treat the exchange-correlation interactions. To describe the strong correlation effects of the electrons around the Cr atoms, the GGA+U method is employed, with an effective Hubbard U_{eff} value of 1.0 eV on the atomic sites. A vacuum layer of 15 Å thickness is included. Lattice relaxation is carried out using a $12 \times 12 \times 1$ Monkhorst-Pack \mathbf{k} -point grid, a plane-wave cutoff energy of 450 eV, and a force convergence criterion of 1 meV/Å.

From first-principles calculations, the band structure and spin polarization of $\text{Cr}_2\text{Ge}_2\text{Te}_6$ can be obtained, as shown in Figs. 2(c) and 2(d). When spin-orbit coupling (SOC) is not considered, the band structure is spin-resolved, and there is no coupling between different spin states. Once considering SOC, the electronic spin polarization is no longer discrete. Figure 2(d) shows the band structure with SOC and the magnitude of the z-component spin polarization. The originally orthogonal spin states open a gap at the band crossings, the dipoles are allowed to form between different spin states. As Figs. 2(c) and 2(d) show, the band structure modulation induced by SOC directly affects the polarization path of dipoles [148]. Through the intraband transport, polarization currents formed by dipoles are generated between the opposite spin states, which mainly occupy low-energy region below the bandgap.

We focus on the elliptical dichroism of harmonic spectra induced by the intrinsic magnetism of materials. A mid-infrared laser field with the wavelength of 9100 nm, the field strength of 2.57 MV/cm, and the full width at half maximum of around 7 cycles is used. In the calculation, we use Wannier90 to construct the maximally localized Wannier functions (MLWF) to obtain transition dipole moments [32-34]. Semiconductor Bloch equation is used here [35-39]. We consider the superposition of harmonic contributions of two sets of spin-up and spin-down bands for the case without SOC. Four valence bands and four conduction bands participating in the simulation has been tested to converge.

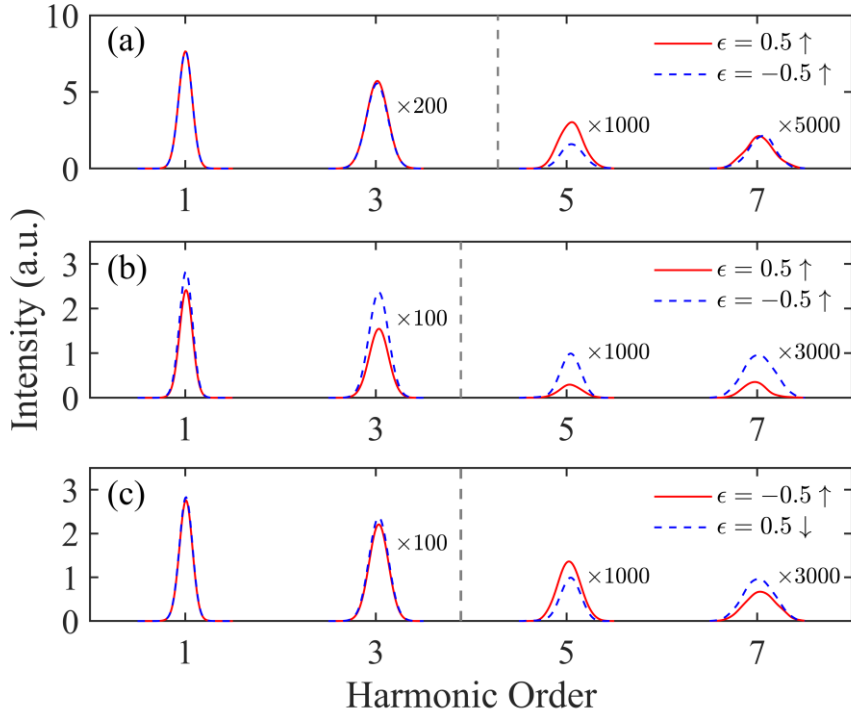


FIG. 3. Harmonic elliptical dichroism of bilayer $\text{Cr}_2\text{Ge}_2\text{Te}_6$ (a) without SOC and (b,c) with SOC. The laser ellipticity $\epsilon = \pm 0.5$ is used. The gray dotted lines mark the bandgap energy. Arrows denote the spin polarization of the crystal.

Figure 3 shows the harmonics of $\text{Cr}_2\text{Ge}_2\text{Te}_6$ under laser fields with opposite helicity. There are only odd harmonics due to the inversion symmetry of this material. The harmonic elliptical dichroism below the bandgap energy is almost negligible without considering SOC, but becomes highly significant when SOC is taken into account. Overall dependence of harmonic intensity on laser ellipticities is shown in the Supplemental Material (SM). In the absence of SOC, the electronic orbital wavefunctions do not contain information about the electron spin, and which retain time-reversal symmetry. So there is no magnetic circular dichroism of harmonics between the spin-up and spin-down polarization cases without SOC (see SM). Upon introducing SOC, the spin magnetic moment disrupts the time-reversal symmetry of the orbital wavefunctions, and the HG appear magnetic circular dichroism, which can also be effectively detected in the harmonic elliptical dichroism spectra without applied magnetic field.

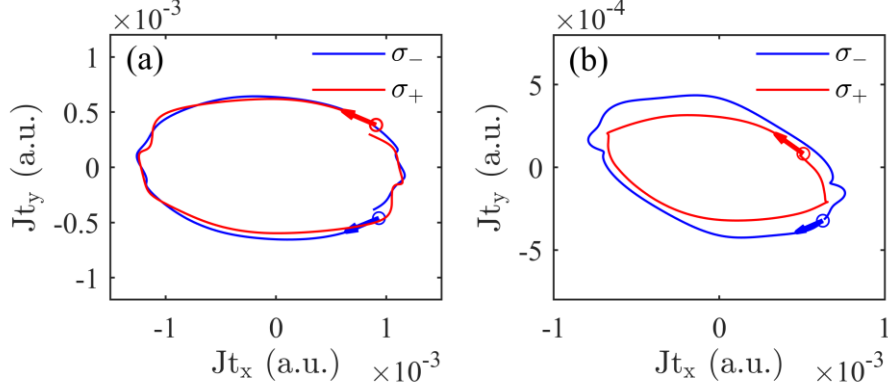


FIG. 4. In-plane low-frequency photocurrent of bilayer $\text{Cr}_2\text{Ge}_2\text{Te}_6$ (a) without SOC and (b) with SOC. The driving laser ellipticity is ± 0.5 , the directions of currents flow over time are denoted by arrows.

We can go back to the photocurrent to confirm the origin of harmonic elliptical dichroism. In the absence of SOC [Fig. 4(a)], the low-frequency (below gap) current driven by opposite helicity lasers are almost uniform, obeying $\mathbf{J}_{\sigma_+}(t) = -\mathbf{J}_{\sigma_-}(-t)$. The

time interval plotted here is $\left[-\frac{T_0}{2}, \frac{T_0}{2}\right]$, T_0 is a single cycle. When the time is reversed, the photocurrent will flow along the opposite direction. However, in Fig. 4(b), the involvement of SOC clearly introduces an additional inconsistent distribution between photocurrents driving by opposite helicity lasers.

This inconsistency can be attributed to the broken symmetry of the polarization current phase. $\text{Cr}_2\text{Ge}_2\text{Te}_6$ has inversion symmetry and 3-fold rotation symmetry, which are not broken by the magnetic structure, so its band structure, transition dipole moment amplitudes in \mathbf{k} space always satisfy symmetry requirement. The consistency of the low-frequency harmonics mentioned above obviously does not come from crystal point-group symmetry. Exactly, due to the disruption of the time-reversal symmetry of the band wavefunctions by SOC, the symmetry of shift phase and ΔTDP related to the band wavefunctions is broken. Thus, the phase of the polarization currents mentioned above but formed by different spin states is no longer symmetric under time reversal, which could be called a magnetic phase. i.e.,

$$\hat{T}S_{\uparrow\downarrow,\sigma_{\pm}}[\mathbf{k}(t), t, t']\hat{T}^{\dagger} \rightarrow S_{\downarrow\uparrow,\sigma_{\mp}}[-\mathbf{k}(t), -t, -t'] \neq -S_{\uparrow\downarrow,\sigma_{\pm}}[\mathbf{k}(t), t, t']. \quad (5)$$

As shown in Fig. 2(c), the polarization rule of dipoles between the same spin states is protected by time-reversal symmetry. The circularly polarized lasers with opposite helicities will generate the consistent low-frequency current at opposite \mathbf{k} points (this can be found as evidences in the monolayer MoS_2 and Weyl semimetal [13,40]). The sole difference between Fig. 2(d) and Fig. 2(c) is that the SOC introduces dipoles between different spin states. These dipoles form polarization currents with asymmetric magnetic phases that induce the elliptical dichroism of the harmonics below the bandgap. Moreover, when we simultaneously flip the helicity of the laser and the spin polarization of the crystal, the consistency reappears due to the overall time-reversal

symmetry between the two laser-crystal systems [see Fig. 3(c)].

In conclusion, we explain the consistency of low harmonic intensities driven by strong lasers with opposite helicities, which results from the time-reversal symmetry of crystals. Breaking the time-reversal symmetry leads to the elliptical dichroism of harmonics, which is effective not only in the linear response but also in the strong-field nonlinear region. The traditional SHG can generally only serve as evidence of the non-centrosymmetric magnetic structure, and it is relatively difficult to determine its accurate origin. Our work extends the MO Faraday or Kerr effect to the nonlinear domain, improving the sensitivity and applicability of magnetic detection methods. The solid-state HG under strong fields carries the characteristic information of the electronic wavefunction, and its magnetic phase can imprint the broken time-reversal symmetry of wavefunctions onto the elliptical dichroism of the harmonic intensity. Due to the pertinence of the time-reversal symmetry breaking, this approach can be applied not only to ferromagnetic materials, but also to antiferromagnetism and altermagnetism. Leveraging the capability of solid-state HG in strong laser fields to probe the point-group symmetry of crystals, it holds further promise to become a powerful tool for retrieving the magnetic point group of crystals.

References

- [1] O. E. Alon, V. Averbukh, and N. Moiseyev, *Physical Review Letters* **80**, 3743 (1998).
- [2] O. Neufeld, D. Podolsky, and O. Cohen, *Nature Communications* **10**, 405 (2019).
- [3] C. Qian, S. Jiang, T. Wu, H. Weng, C. Yu, and R. Lu, *Physical Review B* **109**, 205401 (2024).
- [4] T. Morimoto and N. Nagaosa, *Science advances* **2**, e1501524 (2016).
- [5] Y.-Y. Lv *et al.*, *Nature Communications* **12**, 6437 (2021).
- [6] R. E. F. Silva, Á. Jiménez-Galán, B. Amorim, O. Smirnova, and M. Ivanov, *Nature Photonics* **13**, 849 (2019).
- [7] C. Qian, C. Yu, S. Jiang, T. Zhang, J. Gao, S. Shi, H. Pi, H. Weng, and R. Lu, *Physical Review X* **12**, 021030 (2022).
- [8] Y. Murakami, M. Eckstein, and P. Werner, *Physical Review Letters* **121**, 057405 (2018).
- [9] R. E. F. Silva, I. V. Blinov, A. N. Rubtsov, O. Smirnova, and M. Ivanov, *Nature Photonics* **12**, 266 (2018).
- [10] C. Shao, H. Lu, X. Zhang, C. Yu, T. Tohyama, and R. Lu, *Physical Review Letters* **128**, 047401 (2022).
- [11] D. Xiao, G.-B. Liu, W. Feng, X. Xu, and W. Yao, *Physical review letters* **108**, 196802 (2012).
- [12] O. Neufeld, D. Ayuso, P. Decleva, M. Y. Ivanov, O. Smirnova, and O. Cohen, *Physical Review X* **9**, 031002 (2019).
- [13] R. Yu, H. Weng, Z. Fang, H. Ding, and X. Dai, *Physical Review B* **93**, 205133 (2016).
- [14] Q. Ma *et al.*, *Nature Physics* **13**, 842 (2017).
- [15] G. P. Zhang, M. S. Si, M. Murakami, Y. H. Bai, and T. F. George, *Nature Communications* **9**, 3031 (2018).
- [16] J. Liu *et al.*, *Journal of the American Chemical Society* **138**, 5441 (2016).
- [17] F. Willems *et al.*, *Physical Review B* **92**, 220405 (2015).
- [18] T. Fan *et al.*, *Proceedings of the National Academy of Sciences* **112**, 14206 (2015).

- [19] C. La-O-Vorakiat *et al.*, Physical Review Letters **103**, 257402 (2009).
- [20] C. Gong *et al.*, Nature **546**, 265 (2017).
- [21] P. Němec, M. Fiebig, T. Kampfrath, and A. V. Kimel, Nature Physics **14**, 229 (2018).
- [22] B. Huang *et al.*, Nature **546**, 270 (2017).
- [23] Z. Sun *et al.*, Nature **572**, 497 (2019).
- [24] M. Fiebig, V. V. Pavlov, and R. V. Pisarev, JOSA B **22**, 96 (2005).
- [25] J. E. Sipe and A. I. Shkrebtii, Physical Review B **61**, 5337 (2000).
- [26] M. Fiebig, D. Fröhlich, B. B. Krichevstov, and R. V. Pisarev, Physical Review Letters **73**, 2127 (1994).
- [27] H. Pi, S. Zhang, and H. Weng, Quantum Frontiers **2**, 6 (2023).
- [28] N. Tancogne-Dejean, O. D. Mücke, F. X. Kärtner, and A. Rubio, Nature Communications **8**, 745 (2017).
- [29] N. Klemke *et al.*, Nature Communications **10**, 1319 (2019).
- [30] W.-n. Ren, K.-j. Jin, J.-s. Wang, C. Ge, E.-J. Guo, C. Ma, C. Wang, and X. Xu, Scientific Reports **11**, 2744 (2021).
- [31] G. Kresse and J. Furthmüller, Computational materials science **6**, 15 (1996).
- [32] A. A. Mostofi, J. R. Yates, Y.-S. Lee, I. Souza, D. Vanderbilt, and N. Marzari, Computer physics communications **178**, 685 (2008).
- [33] R. E. F. Silva, F. Martín, and M. Ivanov, Physical Review B **100**, 195201 (2019).
- [34] Q. Wu, S. Zhang, H.-F. Song, M. Troyer, and A. A. Soluyanov, Computer Physics Communications **224**, 405 (2018).
- [35] J. Wilhelm, P. Grössing, A. Seith, J. Crewse, M. Nitsch, L. Weigl, C. Schmid, and F. Evers, Physical Review B **103**, 125419 (2021).
- [36] D. Golde, T. Meier, and S. W. Koch, Physical Review B **77**, 075330 (2008).
- [37] G. Vampa, C. R. McDonald, G. Orlando, D. D. Klug, P. B. Corkum, and T. Brabec, Physical Review Letters **113**, 073901 (2014).
- [38] J. Li, X. Zhang, S. Fu, Y. Feng, B. Hu, and H. Du, Physical Review A **100**, 043404 (2019).
- [39] L. Yue and M. B. Gaarde, Physical Review A **101**, 053411 (2020).
- [40] D. Xiao, G.-B. Liu, W. Feng, X. Xu, and W. Yao, Physical Review Letters **108**, 196802 (2012).

Supplemental Material

Here, we show the laser ellipticity dependence of harmonic intensity [see Fig. S1]. For the 1st and 3rd HG, their intensities are symmetric with respect to the laser ellipticity $\epsilon = 0$, when spin-orbit coupling (SOC) is not considered. After taking into account the SOC, the broken time-reversal symmetry in the spin space is coupled to the orbital wavefunctions. Through the electric dipole effect, the symmetry breaking can be reflected in the elliptical dichroism of the harmonics. Our discussion is not limited to the 1st and 3rd harmonics, but applies to the harmonics below the bandgap energy. The 5th harmonic is slightly above the bandgap, so it will also deviate from the symmetric behavior without SOC. If symmetry allows, the 2nd harmonic is also within the scope of our theory.

Magnetic circular dichroism measurement can provide good time and energy resolution for the magnetization process of materials. If the material have no SOC, there

should be no magnetic circular dichroism of harmonics between the spin-up and spin-down polarization cases, which means its orbital wavefunctions still maintain the time-reversal symmetry. Upon introducing SOC, the HG appear magnetic circular dichroism, which indicates the spin magnetic moment disrupts the time-reversal symmetry of the orbital wavefunctions [see Fig. S2].

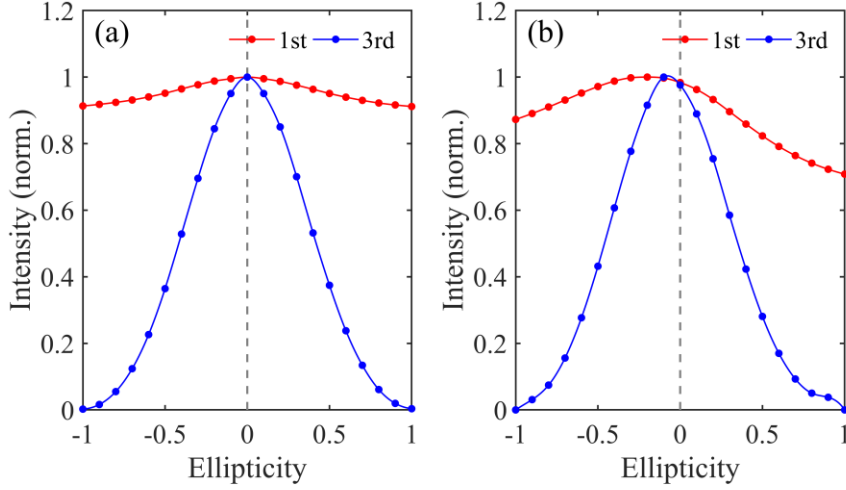


FIG. S1. Ellipticity dependence of harmonic intensity from bilayer $\text{Cr}_2\text{Ge}_2\text{Te}_6$ (a) without SOC and (b) with SOC.

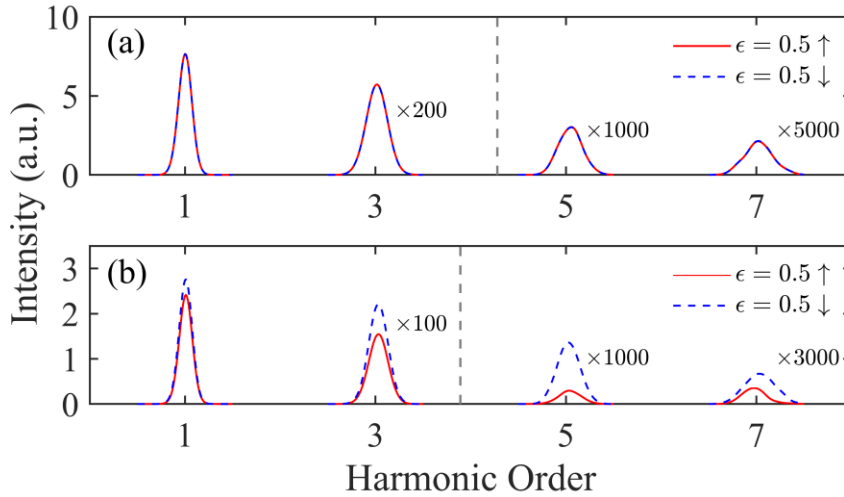


FIG. S2. Magnetic circular dichroism of harmonic intensities from bilayer $\text{Cr}_2\text{Ge}_2\text{Te}_6$ (a) without SOC and (b) with SOC. The laser ellipticity $\epsilon = 0.5$ is used.